HHS Public Access

Author manuscript

J Biomed Nanotechnol. Author manuscript; available in PMC 2017 March 01.

Published in final edited form as:

J Biomed Nanotechnol. 2016 March ; 12(3): 435–449. doi:10.1166/jbn.2016.2195.

Gold Nanosphere Gated Mesoporous Silica Nanoparticle Responsive to Near-Infrared Light and Redox Potential as a Theranostic Platform for Cancer Therapy

Bei Cheng[†], **Huacheng He**[†], **Tao Huang**[§], **Stuart S. Berr**[§], **Jiang He**[§], **Daping Fan**[‖], **Jiajia Zhang**[‡], and **Peisheng Xu**[†]

Peisheng Xu: xup@sccp.sc.edu

[†]Department of Drug Discovery and Biomedical Sciences, University of South Carolina, Columbia, SC 29208, USA

[§]Department of Radiology and Medical Imaging, University of Virginia, Charlottesville, VA 22908, USA

[‖]Department of Cell Biology and Anatomy, University of South Carolina School of Medicine, Columbia, SC 29209, USA

[‡]Department of Epidemiology and Biostatistics, University of South Carolina, Columbia, SC 29208, USA

Abstract

A gold/mesoporous silica hybrid nanoparticle (GoMe), which possesses the best of both conventional gold nanoparticles and mesoporous silica nanoparticles, such as excellent photothermal converting ability as well as high drug loading capacity and triggerable drug release, has been developed. In contrast to gold nanorod and other heat generating gold nanoparticles, GoMe is photothermal stable and can be repetitively activated through NIR irradiation. Doxorubicin loaded GoMe (DOX@GoMe) is sensitive to both NIR irradiation and intracellularly elevated redox potential. DOX@GoMe coupled with NIR irradiation exhibits a synergistic effect of photothermal therapy and chemotherapy in killing cancer cells. Furthermore, ^{64}Cu-labeled GoMe can successfully detect the existence of clinically relevant spontaneous lung tumors in a urethane-induced lung cancer mouse model through PET imaging. Altogether, GoMe can be utilized as an effective theranostic platform for cancer therapy.

Graphical abstract

We developed a gold/mesoporous silica hybrid nanoparticle (GoMe) for cancer detection and treatment. GoMe is sensitive to NIR irradiation and elevated redox potential, and showing synergistic chemo-thermal therapy effects.

Correspondence to: Peisheng Xu, xup@sccp.sc.edu.

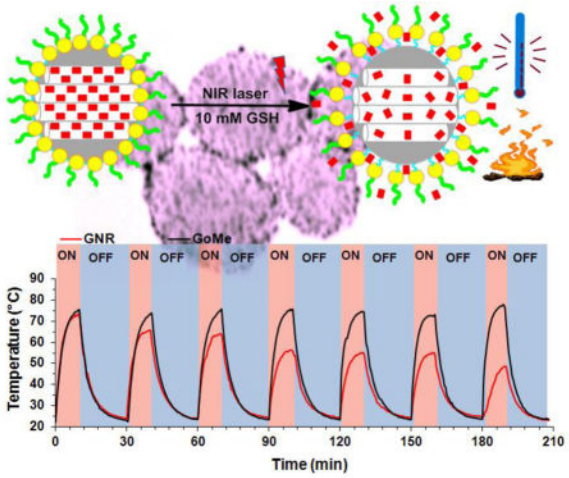

Keywords

gold nanoparticle; mesoporous silica nanoparticle; redox responsive; photothermal therapy; cancer detection

1. Introduction

Gold nanoparticles, including gold nanosphere (GNS), gold nanorod (GNR), gold nanoshell (GNSH), and gold nanocage (GNC), have attracted tremendous attentions during the past decade and have been extensively explored in biomedical applications, such as drug and gene delivery, disease detection, treatment, and response monitoring, due to their excellent biocompatibility, and easy surface modification.[1,2] Upon irradiation, gold nanoparticles generate heat attributable to the localized surface plasmon resonance (LSPR) phenomenon.[3,4] By manipulating their shape, size, and geometry, the LSPR peak of GNR, GNSH, and GNC can be tuned to near-infrared (NIR) region, also called tissue transparent window (650–900 nm), within which light can penetrate deeply.[5] Because of that, upon NIR irradiation, these gold nanoparticles generate heat and can be applied for photothermal therapy.[3,6–12] Although gold nanoparticles have been evaluated in numerous systems and proven to be promising in photothermal therapy and drug delivery, there are several intrinsic properties limiting their translation from bench to clinical practice. First, due to their poor photothermal stability, traditional gold nanoparticles gradually lose their photothermal converting capacity upon repetitive NIR irradiation. It has been well documented that the shape and extinction of GNR changed after NIR laser irradiation and resulted in lower heat generating capacity after each heating/cooling cycle.[13] Similar scenarios also have been observed in GNSH and GNC if the generated heat could not be dissipated to their surrounding environment.[14,15] In addition, except GNCs, other gold nanoparticles are not good drug carriers either due to limited drug loading capacity or poorly controlled drug release profile.[16,17] Furthermore, although tremendous efforts have been devoted, how to effectively integrate both photothermal therapy and chemotherapy modules into one system remains a challenge, especially when repetitive activation is needed.

Similar as gold nanoparticles, last decade also witnessed increasing attention gained by mesoporous silica nanoparticle (MSN) due to its high and versatile drug loading capacity as well as good biocompatibility. Numerous MSN based carrier systems have been developed for the delivery of drugs, peptides, DNAs, and siRNAs. To better control the release kinetics of their payloads, many gatekeepers have been explored, such as polyelectrolytes,[18,19] macrocyclic organic molecules,[20–22] and inorganic nanoparticles.[23,24] Generally, these MSN delivery systems are responsive only to the changes in the physiological environment, such as pH and redox potential. Once the MSN is administrated *in vivo*, the drug release profile will be out of the control of the clinician and be totally relying on its fabrication method and biodistribution. To overcome the limitations of existing gold nanoparticles and MSNs in photothermal therapy and drug delivery, we developed a gold/mesoporous silica hybrid nanoparticle (GoMe) by conjugating gold nanospheres (GNS) onto the surface of MSN (Figure 1A) to take advantage of the best of both worlds.

2. Material and Methods

2.1. Materials

Terraethylorthosilicate (TEOS), (3-Mercaptopropyl)trimethoxysilan) (MPTMS), Hexadecyltrimethyl ammonium bromide (CTAB), sodium hydroxide (NaOH), Pluronic® F-127, Ammonium nitrate, methanol, gold chloride trihydrate, cysteamine hydrochloride, 2,2′-dipyridyl disulfide, triethylamine (TEA), Doxorubicin (DOX), and sodium borohydride ($NaBH_4$) were purchased from Sigma-Aldrich. PEG2000-SH was purchased from Laysan Bio. Ethanol and acetic acid were acquired from Fisher Scientific.

2.2. Synthesis of mesoporous silica nanoparticles (MSN)

The MSN was synthesized in a dual surfactant system using a classic fast self-assembling method containing both the cationic surfactant cetyl trimethylammonium bromide (CTAB) and non-ionic surfactant triblock polymer F 127 to obtain a good suspending nano-sized MSN. In a typical synthesis, CTAB (50 mg) and F 127 (40 mg) were dissolved in 24 mL DI water. After that, NaOH aqueous solution (175 μL, 2M) was added into the above mixture. The reactants were heated to 80 °C with vigorous stirring for 30 min. TEOS (200 μL) was added dropwise to the above solution followed by 3-Mercaptopropyl trimethoxysilan (MPTMS, 20 μL). A white precipitant was formed after a few minutes and the mixtures were allowed to stir for 2 h at 80 °C. The crude product was collected by centrifugation at 16,000 rcf for 15 min. CTAB was removed through ion exchange by washing in ethanol solution of NH_4NO_3 at 50 °C. This process was repeated for 3 times, followed by extensively washing with ethanol and the purified product was stored at 4 °C in ethanol solution.

2.3. Synthesis of PEG stabilized gold nanosphere (PEG-GNS)

The super-stable gold nanosphere was synthesized according to literature with minor modification.[25] Briefly, gold (III) chloride trihydrate (12 mg) was first dissolved in 18 mL isopropyl alcohol and followed with the addition of 0.2 mL acetic acid. Thiolated polyethylene glycol (PEG-SH, M_W=2000 Da) (15.24 mg in 2 mL isopropyl alcohol) was added into the gold alcohol solution. The mixture was stirred for 1 h at room temperature

following the addition of sodium borohydride (37.84 mg in 1.5 mL methanol). The reaction mixture was stirred vigorously overnight at room temperature. After overnight reaction, the mixture was centrifuged for 30 min (2500 rcf) to remove large particles. The resulting supernatant was precipitated in hexane. The precipitant was re-dispersed in 5 mL DI water. To remove free PEG-SH from gold nanoparticle, the PEG-GNS was purified by repeatedly washing with water in a Millipore Centricon (MW CO=10,000 Da). The successful anchoring of PEG-SH onto gold nanosphere was confirmed by ^{1}H-NMR (Figure 2A). The zeta potential of PEG-GNS was measured by Zetasizer Nano ZS (Malvern) and showed a near neutral potential (−8.65 mV), which further confirmed the successful coating of PEG onto the GNS. The morphology of PEG-GNS was confirmed by TEM. The UV-Vis spectrum of PEG-GNS was recorded by UV-Vis spectrophotometer (DU®650 Spectrophotometer, Beckman Coulter, USA), which showed an absorbance peak at 510 nm.

2.4. Synthesis of 2-(pyridin-2-yldisulfanyl)ethyl acrylate modified GNS (PDA-GNS)

PDA-GNS was synthesized in a two-step procedure by conjugating PEG-GNS with cysteamine first, followed by reacting with 2-(pyridin-2-yldisulfanyl)ethyl acrylate (PDA) through Michael addition reaction. Briefly, the PEG-GNS synthesized above was dispersed in 10 mL DI water, and then cysteamine (0.216 mg in 40 μL H_2O) was added. The mixture was kept stirring at room temperature. After 24 h of stirring, the reaction solution was loaded to a Millipore Centricon (MWCO=10,000 Da) and repeatedly washed by centrifugation to remove un-reacted cysteamine. The successful conjugating of cysteamine was confirmed by zeta potential measurement, which showed a highly positive charge (+27 mV) on the GNS surface. The surface amine concentration was further measured by TNBSA assay, which also proved the successful replacement of PEG by cysteamine. The GNS concentration was determined by calculating UV-Vis absorbance according to literature.[2] The result showed that there were around 1000–NH_2 groups located on the surface of each GNS. After that, PDA was conjugated to the GNS by reacting with amine groups *via* Michael addition reaction. Typically, cysteamine modified GNS was dispersed in 500 μL of DMSO, and triethylamine (0.265 μL in 26.5 μL DMSO) was added, following the addition of PDA (0.459 mg in 50 μL DMSO). The ratio between –NH_2 and PDA was optimized at 2:1 since a higher -NH_2 to PDA ratio could easily result in GNS aggregation during the post-purification process. The reaction mixture was purged with nitrogen and then kept at 50 °C for 24 h. The resulting PDA-GNS was precipitated in cold ether for three times to remove unreacted PDA and finally re-dispersed in 2 mL DI water. The successful conjugation of PDA was confirmed by UV-Vis spectrum (Figure 2B). PDA-GNS showed a PDA characteristic peak around 375 nm after reacting with dithiothreitol (DTT). The PDA concentration of PDA-GNS was measured by DTNB assay, which proved that about 200 PDA was anchored to each GNS.

2.5. Encapsulation of doxorubicin (DOX) into MSN

To load DOX into MSN, DOX•HCl was firstly converted to its base form by mixing with triethylamine for 30 min. In a typical synthesis batch, 10 mg DOX was added to 18.6 mg MSN and the mixture was sonicated for 30 min to obtain a uniform dispersion. The mixture was stirred at room temperature for 24 h and the unloaded DOX was removed by washing with DI water twice. It was denoted as DOX@MSN. The loading efficiency of DOX was

quantified by a fluorospectrometer (Beckman Coulter, DTX 880). Different loading of DOX can be simply tuned by changing the ratio between DOX and MSN. In this experiment, the highest drug loading content of DOX in DOX@MSN reached 28%.

2.6. Fabrication of GNS decorated MSN (GoMe)

GNS was grafted onto MSN through thiol-disulfide exchange reaction. MSN (200 μg in 200 μL) aqueous solution was added to 2 mL PDA-GNS aqueous suspension while stirring. The mixture was allowed to react at room temperature for 24 h, and then washed three times with DI water. The final product was collected by centrifugation. The size and morphology of the GoMe was determined by TEM.

2.7. Photothermal stability assay

The repetitive laser irradiation experiments were carried out to test the photothermal stability of GoMe and gold-nanorod, which is critical for multiple photothermal treatments. Firstly, the concentration of GoMe and gold nanorod were adjusted to generate equal increment in temperature upon the same intensity of laser irradiation. The GoMe suspension was irradiated by a 808 nm laser for 10 min (Scorpius D-700 laser, 2.83 W/cm^2). The temperature of the nano-suspension was monitored with a FLIR i7 thermal imaging camera and recorded every 30 sec. Both the GoMe and the GNR (maximum absorbance peak at 804 nm) were undergone 6 continuous laser irradiation cycles (10 min irradiation and 20 min cooling). The 7th irradiation was applied 24 h after the 6th cycle. The UV-vis spectra and TEM images were recorded to reveal the change during the repeating cycles. The photothermal stability of GoMe in reducing environment was further investigated by dispersing GoMe in DI water supplemented with 10 mM GSH.

2.8. Laser irradiation triggered release of GoMe

To evaluate the responsiveness of GoMe to NIR light, 20 μL of GoMe containing 4 μg of DOX was diluted with 250 μL DI water. The GoMe suspension was incubated at 37 °C to carry out the release study. GoMe nano-suspension was centrifuged at 1, 2, 4, 6, 8, 12, and 24 h at 16,000 rcf for 10 min to separate released DOX from GoMe particles. After that, the same amount of fresh medium was added to resuspend the GoMe pellet. At 24 h post the start of the releasing experiment, the GoMe suspension was irradiated by a 808 nm laser for 10 min (2.83 W/cm^2). Sample was collected immediately by centrifugation after the irradiation. The sample was then incubated at 37 °C followed by sampling twice (at 1 h intervals), and then incubated till the next 24 h point. The whole release process was continued for 4 days. The amount of DOX in the supernatant was determined by a fluorospectrometer (Beckman Coulter DTX 880, excitation: 485 nm and emission: 545 nm).

2.9. GNS decorating density effect assay

The effects of different GNS density on a single MSN were explored by examining the product of the reaction between GNS and MSN at different time intervals. The reaction was carried out in a transparent 2.5 mL spectrophotometer cuvette. The UV absorbance spectrum was recorded directly as the reaction proceeding, while the photothermal converting capacity of the mixture was examined by irradiating the diluted reaction mixture with a 808

nm laser. The reaction was also monitored by observing the morphology of GoMe with the help of TEM.

2.10. Cellular internalization assay

The A2058 cell, a human melanoma cell line, was cultured in Dulbecco's modification of eagle medium (Corning, Manassas, VA) supplemented with 10% FBS and 1% penicillin-streptomycin (Life Technology, Grand Island, NY) at 37 °C in 5% humidified CO_2 atmosphere. Cells were seeded in 35 mm petri dishes with a density of 200,000 cells/petri dish. After overnight incubation, 5 μM DOX@GoMe was added and continued incubation for another 3 h. Cells were washed once with complete medium and then stained with Hoechst 33342, followed by confocal microscopy imaging (LSM 700, Zeiss) and dark field microscopy imaging (Leica DM6000 M).

2.11. Live/dead cell assay after photothermal therapy

The photothermal effect of GoMe in cell culture medium was evaluated in a 96-well plate. GoMe of different concentrations were added to each well containing 100 μL complete medium. The resulting GoMe nano-suspension was irradiated with NIR laser (808 nm, 2.83 W/cm^2) for 10 min at predesigned time intervals and its temperature was monitored with a FLIR i7 thermal imaging camera and recorded every 1 min. To visualize the effect of laser irradiation on the cell death, Live/Dead cell imaging kit (Molecular Probe®) was used. 10,000 cells were seeded in 96-well plate and incubated at 37 °C in 5% CO_2 overnight. Blank GoMe (1 μM or 5 μM) was added and incubated for 2 h. For GoMe treated groups, a 808 nm laser was used to irradiate cells for 10 min, while others had no laser treatment. Cells were kept in the incubator for 2 h and stained with Live/Dead cell imaging kit according to the manufacturer's instruction. Each well was imaged from 5 different positions (top, bottom, left, right and middle) with fluorescent microscopy (Axiovert 200, Carl Zeiss) under 20 × magnification using FITC and Texas red channels.

2.12. Cytotoxicity assay

For cell viability assays, A2058 cells were seeded in a 96-well plate (10,000 cells/well) and incubated at 37 °C in 5% CO_2 overnight. DOX, MSN, DOX@MSN, GoMe, and DOX@GoMe were diluted with complete medium to achieve targeted concentrations. After 24 h of incubation, GoMe and DOX@GoMe irradiation groups were exposed to 808 nm laser irradiation for 10 min. The cells were allowed to grow overnight and then added with MTT reagent. MTT stop solution was added after 4 h of incubation to dissolve MTT formazan crystals. The optical density of the medium was measured using a microplate reader (ELX808, Bio-Tech Instrument, Inc.) at $\lambda = 595$ nm.

2.13. ^{64}Cu Radiolabeling of GoMe Nanoparticle

DOTA was conjugated onto GoMe nanoparticles by adding maleimido-mono-amide-DOTA (20 mM, 50 μL in DMSO) to 1 mg GoMe aqueous solution (1 mg/ml). After 6 h of reaction at room temperature, the free DOTA was separated from GoMe by centrifugation and washing with DI water twice. The resulting pellet was re-suspended in 1 ml DI water. GoMe nanoparticles were further radiolabeled by ^{64}Cu via the DOTA chelator as previously

reported.[26] The radiolabeling was accomplished by addition of 1.0–1.5 mCi of $^{64}CuCl_2$ in 0.1 M HCl (University of Wisconsin) to a mixture of 50 μL 0.1 N ammonium acetate (pH 5.5) buffer and 150–200 μL of the nanoparticles suspension, followed by incubation at 37°C for 30 min. The radiolabeled nanoparticles were collected into 300–400 μL of phosphate buffered saline by centrifugation.

2.14. Animal model establishment

All experiments were carried out under protocols approved by the Institutional Animal Care and Use Committee. Our mouse model was based on one reported by Berr's group.[26] Female FVB mice (Jackson Laboratory) aged 6–8 weeks received weekly intraperitoneal (IP) injections of 1 mg urethane/g body weight dissolved in sterile 0.9% NaCl. Twenty weeks after the initial urethane injection, MRI was used to verify lung tumor presence. PET imaging was performed when at least one lung tumor reached 1.5 mm in diameter.

2.15. MRI and PET Animal imaging

Twenty-four weeks after urethane treatment, lung tumor bearing mice were first imaged on a 7 Tesla ClinScan MRI system (Bruker BioSpin Corporation, Billerica, MA), Inc., Palo Alto, CA). MRI were acquired with a cardiac and respiratory gated, multi-slice, spin-echo sequence developed in our lab with the following parameters: field of view 30 mm, effective matrix = 192 × 192 zero-filled to 256 × 256, slice thickness 0.7 mm, TR was a function of the breathing cycle and averaged to about 1 second. The TE was 11ms, the number of averages was 4, the number of slices was 15 with a gap equal to 0.7mm between slices to avoid crosstalk. The slice stack was moved by 0.7mm and 15 other interleaved slices were acquired. Gadolinium-DTPA contrast agent (Magnevist; Bayer Schering Pharma, Berlin, Germany) was injected at a dose of 50 mmol/kg body weight in the hind leg muscle. Before PET imaging, mice were injected with ^{64}Cu-labeled GoMe nanoparticles via the lateral tail vein. Each mouse received 500–750 μCi of ^{64}Cu for a total volume of 150–200 μL. Mice were imaged using a Focus 120 PET scanner (Positron Emission Tomography) (Siemens, Knoxville, TN) at 6 h and 20 h post administration. During the 40 min PET acquisition, anesthesia was maintained using 1.25% isoflurane in O_2 inhaled through a nose cone. Heart rate, respiration, and rectal temperature were monitored (SAII, Stony Brook, NY). PET data were reconstructed using OSEM algorithm with 2 iterations and 12 subsets followed by MAP algorithm (18 iterations). The reconstructed image (not corrected for attenuation) was composed of 95 axial slices of thickness 0.79 mm with an in-plane voxel dimension of 0.4 mm × 0.4 mm (128 × 128 pixels).

3. Results

3.1. Gold/mesoporous silica hybrid nanoparticle (GoMe) fabrication

Thiolated MSN was fabricated by the co-condensation of (3-mercaptopropyl) trimethoxysilane (MPTMS) with tetraethyl orthosilicate (TEOS) as described by the literature.[27] TEM revealed that most MSNs are in spherical or oval shape with a size of 50.87 ± 10.69 nm (Figure 1B). The N_2 sorption measurement revealed that the pore size of MSN is about 2–3 nm (Figure 3), with a surface area of 858 m^2/g. The accessible thiol groups on the MSN were quantified with Ellman's reagent using cysteine as a reference

standard. The amount of thiol groups in MSNs was 31 μmol/g. The super stable gold nanosphere (GNS) was synthesized according to literature with minor modification.[25] Thiolated polyethylene glycol (PEG-SH, Mw=2000 Da) was added into the gold isopropanol alcohol solution before the formation of GNS. The resulting PEG-GNS was spherical with a diameter of 3.93 ± 0.70 nm (Figure 1C). The resulting PEG-GNS was further functionalized through a two-step procedure by conjugating PEG-GNS with cysteamine first, followed by reacting with homemade 2-(pyridin-2-yldisulfanyl)ethyl acrylate (PDA) *via* Michael addition reaction to yield PDA-GNS as shown in Figure 1A. DTNB assay revealed that about 200 PDA molecules were anchored to each GNS. PDA-GNS was grafted onto MSN through thiol-disulfide exchange reaction (Figure 1A) by simply mixing PDA-GNS and thiolated MSN in DI water for 24 h. TEM was employed to investigate the assembly between GNSs and MSNs. Figure 1D showed that most GNSs were evenly attached to the surface of MSNs. This gold nanosphere/mesoporous silica nanoparticle hybrid assembly was named as GoMe. To our surprise, only a few free GNSs were detected after the reaction, indicating the high efficiency of the conjugation reaction. The success of grafting of GNS onto MSN was further confirmed by SEM image and SEM/EDX analysis. The evenly distributed small spherical dots on the bigger balls (Figure 4) and the presence of Au element (Figure 5B) indicated that GoMe had a structure as shown in Figure 1A. Zetasizer found that GoMe carried slightly negative surface charge (−5.92 ± 0.75 mV, Figure 6). Due to the existence of PEG outer layer, GoMe was stable in culture medium containing 10% FBS (Figure 7), and no obvious size change and aggregation were observed after two months of incubation. The size of GoMe determined by dynamic light scattering (DLS, 141.7 nm) was larger than that observed by TEM (54.71 ± 9.63 nm), which is because that TEM measures physical size of the dried particles while DLS measures their hydrodynamic diameter (including the water layer surrounding the particle).

3.2. Photothermal property characterization

To monitor the fabrication progress of GoMe, UV-Vis spectrophotometer was employed by recording the absorbance from 400 to 1000 nm during the reaction. Figure 8A showed that the absorbance peak of the reaction mixture at 524 nm decreased over time and slightly shifted to long wavelength direction, while its absorbance in the NIR region gradually increased. To evaluate the photothermal properties of the reaction mixture changing with the progress of the reaction, the reaction suspension was irradiated with NIR laser (808 nm, 2.83 W/cm^2) for 10 min at predesigned time intervals and its temperature was monitored with a FLIR i7 thermal imaging camera and recorded every 30 sec. Before the mixing, the aqueous nano-suspension of MSN produced none while GNS produced little heat under the NIR irradiation (Figure 8B). To our surprise, after 12 h of reaction, the temperature of the mixture of MSN and GNS raised 21.2 °C after irradiation (Figure 8B). Furthermore, the longer the reaction time, the higher the temperature reached. The mixture after 24 h of reaction could be heated to 52.8 °C (30 °C increase) upon the same intensity and length of NIR irradiation. The photothermal conversion efficiency of GoMe was 29.65%, which is slightly higher than the reported GNSH (25%) while lower than GNR (50%).[28]

To probe the mechanism for the mixture of GNS and MSN generating heat upon NIR laser irradiation, TEM was employed to observe the morphology change during the reaction. The reaction mixture was centrifuged to remove unconjugated GNS before loaded onto copper grids for TEM observation. Figure 8C showed that GNSs can be conjugated onto MSN within 2 h. Longer reaction time resulted in a higher GNS decorating density on the surface of MSN (Figure 8D and 8E). Altogether, higher decorating density of GNS on GoMe led to a higher absorbance in the NIR region, which opened the window for the biomedical application of GoMe using a NIR laser (Figure 8A). As a consequence, GoMe with higher GNS decorating density produced more heat upon the NIR laser irradiation (Figure 8B). Figure 9 revealed that GoMe exhibited a concentration-dependent photothermal heating effect. Therefore, a desired photothermal heating curve can be achieved by simply tuning the concentration of GoMe.

Photothermal stability is a vital property for the success of photothermal therapy, especially when repetitive treatment is necessary for the management of recurrent cancer. To evaluate the photothermal stability of GoMe, aqueous suspension of GoMe was repetitively irradiated with a 808 nm NIR laser (10 min on and 20 min off) at the light intensity of 2.83 W/cm^2. The temperature of the nano-suspension was monitored as described above. GNR (aspect ratio of 3.89 and peak absorbance of 804 nm) synthesized according to literature was employed as a control.[29] GNR at a concentration that could produce heat to reach similar temperature as that of GoMe was irradiated in parallel. Figure 10 showed that the temperature of both GoMe and GNR suspensions increased rapidly upon laser irradiation and reached 74 °C in 10 min. As expected, the repetitive heating of GNR suspension resulted in decreased peak temperatures, declined from 74 to 65.8 °C during the second heating cycle and further dropped to 48.5 °C after 6 cycles of laser irradiation induced heating/cooling. To our surprise, GoMe suspension could reach the same peak temperature after 6 heating/cooling cycles, and achieved even higher peak temperature after 24 h of resting period, which suggests that GoMe was stable in keeping its photothermal property during laser irradiation induced heating/cooling process. Such stability is critical for certain biomedical applications which require multiple laser irradiations. Since GNSs were grafted onto MSN through disulfide bonds, the photothermal property of GoMe in reducing environment was further investigated. Figure 11 showed that GoMe only slightly decreased its peak temperature in an environment containing 10 mM GSH, suggesting that most of GNSs were still attached to MSN. As we have confirmed that each GNS had 200 thiol reactive PDA groups, it is reasonable to postulate that every GNS was connected with MSN through multiple disulfide bonds. Therefore, at any given time, GSH only cleaved partial of those disulfide bonds for each GNS and loosened the binding between GNS and MSN. More importantly, repetitive heating/cooling in reducing environment did not change its photothermal converting capacity (Figure 11). Therefore, GoMe would retain its competence in generating heat upon NIR irradiation in an intracellular environment, where it has high GSH level.[30–32]

To probe why GoMe was stable during the NIR laser irradiation induced heating/cooling cycles, while GNR was instable, the UV-Vis spectra of GoMe and GNR after each cycle were recorded. The UV-Vis absorbance of GoMe only marginally changed after 6 cycles of heating/cooling (Figure 12A), while the absorbance of GNR significantly diminished in the

NIR region (Figure 12B). To investigate the morphologies of the GNR and GoMe after above treatment, TEM was employed. Figure 12D proved that the morphology of GoMe remained intact after laser irradiation. By contrast, some GNRs changed their shape significantly after 5 cycles of laser irradiation, becoming shorter and fatter or round (Figure 12F). This rod-to-sphere shape transformation was due to the melting of GNR under the extensive heat itself generated.[13] Since gold nanoparticles melt at high temperature and form gold nano-droplet (or so called nanosphere), similar shape transformations also have be documented for gold nanoshells and gold nanocages.[14] As a consequence of losing their original geometries, these gold nanoparticles showed a compromised photothermal property. However, GoMe, which was fabricated from GNS and MSN, kept its shape unchanged, since GNS remained its original spherical after melting. Therefore, GoMe kept its photothermal capacity intact over multiple heating/cooling cycles.

3.3. Drug release kinetics measurement

To investigate whether the decoration of GNS on the surface of MSN could affect the release profile of its payload, anticancer drug doxorubicin (DOX) was adopted as a model drug and loaded into MSN as described by literature.[33] Due to its high surface area and pore volume, GoMe achieved 28% drug loaded content. Because DOX is a potent anticancer drug, DOX loaded GoMe (DOX@GoMe) of 4.58% drug loading content was adopted for the *in vitro* assay. However, in drug release kinetics study, the DOX@GoMe of 28% drug loading content was employed to achieve a more accurate drug release profile.

An ideal drug carrier should be premature-release free before reaching its target. Furthermore, for a desired delivery system, the release of its payload should be either spontaneously responsive to the stimuli from its target or remotely controlled by external signals. To investigate the release kinetics of DOX from GoMe, DOX@GoMe was suspended in phosphate buffer (PBS, pH 7.4) and PBS supplemented with 10 mM GSH to mimic the environments in the circulating blood and cytosol, respectively. Researchers found that surface non-modified MSN can easily aggregate in aqueous medium,[34] which could result in false release profile. For fair comparison, DOX loaded MSN (DOX@MSN) was also stabilized though PEG-SH surface modification. Figure 13A showed that DOX@MSN released more than 28.8% of its payload within 10 h of incubation in PBS, suggesting that unsealed MSN was not a desired carrier. Interestingly, GoMe, MSN decorated with GNS, released much less of DOX (8.3%) within the same period of time, indicating that GNS could serve as a plug to prevent DOX from leaking out from the pores of MSN during circulating in blood stream. Since GNS was conjugated onto the surface of MSN through disulfide bonds, we further investigated the responsiveness of GoMe to reducing environment by dispersing it in PBS supplemented with 10 mM GSH. As expected, GoMe released much more DOX in reducing environment (66.4% of DOX within 24 h) than that in PBS (10.3%), demonstrating that GoMe was a good carrier for intracellular drug delivery. As we already proved that GoMe could efficiently convert NIR laser irradiation into heat, we further investigated the effect of NIR irradiation on drug release by applying irradiation (10 min laser on in every 24 h period) on the GoMe nano-suspension. Remarkably, Figure 13B showed that 10 min of NIR irradiation induced more than 23% immediate DOX release. The removal of laser irradiation promptly slowed down the drug

release. Moreover, the re-introducing of laser irradiation could accelerate drug release repetitively. The first time NIR irradiation triggered more drug release than the later ones, which possibly due to the liberation of drugs bonded on the surface MSN for the first irradiation while later stimuli induced the release of encapsulated drugs from the pores of MSN. This light activable two-stage drug release pattern can be utilized to meet the clinical setting in drug administeration by providing both loading dose and maintenance dose.

3.4. Observation of GoMe by confocal fluorescent and dark-field microscopies

To explore the potential of using GoMe as a carrier to deliver drug into cancer cells, DOX-loaded GoMe was co-incubated with A2058 melanoma cells for 3 h, and then observed with a confocal microscope. The red fluorescence signals in Figure 14F proved that GoMe loaded DOX could effectively enter A2058 cells. To further confirm that GoMe entered cancer cells, the above cells were also observed with a dark-field microscope. Scatter light signals (yellow and red dots) collected inside A2058 cells (Figure 14J) through a dark-field detector proved that GoMe could be taken up by cancer cells.

3.5. Cell killing effect of GoMe

Figure 15 displayed that GoMe raised medium temperature from 21.8 to 34.6 and 50.3 °C within 10 min of laser irradiation at GoMe concentrations corresponding to 1.67 and 5 μM DOX, respectively. Since GoMe could generate heat and raise medium temperature upon NIR laser irradiation, we first investigated its photothermal therapy effect on the cancer cells through Live/Dead cell assay. A2058 cells were co-incubated with blank GoMes at the corresponding DOX concentration of 5 μM and coupled with NIR laser irradiated for 10 min before the Live/Dead cell assay, and then visualized with a fluorescent microscope. As expected, nearly all non-treated cells were stretched and green (Figure 16A). It was also noted that blank GoMe treated cells (Figure 16B) did not show any morphology difference as compared with the non-treated ones, suggesting GoMe itself was not toxic. By contrast, cells treated with blank GoMe and laser irradiation dramatically changed their morphology, showing round shape (Figure 16C). It was also noticed that the cell density in Figure 16C was much lower than the group without receiving laser irradiation, which was due to the detaching of cells as a result of apoptosis and subsequently being removed during the washing procedure. In addition, a significant portion of cells in Figure 16C were stained in red, confirming that GoMe coupled with NIR irradiation could effectively kill cancer cells.

We have confirmed that NIR laser irradiation could trigger the release of DOX from GoMe, and also proved that photothermal effect of blank GoMe could kill cancer cells. To investigate the cell killing efficacy of DOX@GoMe coupled with NIR irradiation, A2058 cells receiving different treatments were analyzed by MTT assay. Due to the potential residual of cetyl trimethylammonium bromide (CTAB) in the MSN, blank GoMe showed some cytotoxicity. As expected, the application of NIR irradiation enhanced the cell killing effect of GoMe (Figure 16D), especially for GoMe at the concentration of 5 μM. Because the capping effect of GNS and consequent slower drug release, DOX@GoMe was less potent than DOX@MSN in killing cancer cells. Furthermore, Figure 16D also evidenced that the DOX@GoMe coupled with NIR irradiation did show superior anticancer efficacy than either GoMe coupled with NIR irradiation or DOX@GoMe alone. Due to the

photothermal effect of GoMe, NIR irradiation of DOX@GoMe could kill cancer cells by the combination effect of photothermal ablation and boosted drug release and subsequent enhanced chemotherapy. It is worth noting that the effect of NIR irradiation only became significant when GoMe concentration reached 2 μM, at which GoMe could generate enough heat to ablate cancer cells and augment drug release. The combination index (CI) analysis further revealed that the combination of DOX@GoMe and NIR irradiation exhibited synergistic effect at the DOX concentration 5 μM (CI value = 0.50).[35] Therefore, to warrant the synergistic effect between DOX@GoMe and NIR irradiation, high retention of DOX@GoMe in the targeted tissue or cells is required.

3.6. In vivo tumor detection

To endow the PET imaging function to GoMe, DOTA was conjugated onto GoMe nanoparticles by adding maleimido-mono-amide-DOTA. With the help of conjugated DOTA, the yield for GoMe ^{64}Cu-labeling was above 98%, which suggests that GoMe is a good carrier for radiopharmaceuticals. To validate that ^{64}Cu-labeled GoMe can be used as a tool for cancer detection, a clinically relevant spontaneous lung tumor model was employed. The 3 small tumors in the lung (previously revealed by a ClinScan MRI system as shown in Figure 17A) were clearly detected by PET at both 6 h (Figure 17B, 17C) and 20 h (Figure 17D) post-administration, suggesting the high retention of GoMe in the tumor, which proved that GoMe is good tool for the cancer detection. Similar as other nanoparticles, significant amount of GoMe nanoparticles accumulated in liver and spleen as shown in the PET images. The increase of PET signals in the abdomen (colon and rectum) from 6 h to 20 h revealed the rout for GoMe to be cleared from the body.

4. Discussion

Various gold/silica hybrid nanoparticles have been explored as tools for bioimaging and drug carrier. Lee et al. revealed that α-synuclein-coated gold nanoparticle decorated MSN could release its payloads upon the intracellular Ca^{2+} stimulus.[36] Aznar et al. developed a gold/MSN hybrid system through the formation of boronate esters. Due to the hydrolysis of boroester bonds at acidic pH and light induced heat, low pH and light can be used to trigger the release of its cargo.[23] In addition, Sharma et al. also found that gold nanoparticle coated silica nanoparticles could produce strong signals for magnetic resonance imaging (MRI) and photoacoustic tomography (PAT).[37] In our design, gold nanospheres were grafted onto the surface of MSN through disulfide bonds, which endowed the intracellular redox potential responsiveness to GoMe. The surface-assembled GNS can be considered as a structure well-defined assembly of “chainlike gold nanoparticles”,[38] or a discontinuous form of gold nanoshell, both of them can efficiently generate heat upon NIR irradiation. In contrast to its continuous counterpart, GoMe kept its original shape after NIR irradiation due to the distance between each GNS and the support of MSN. Consequently, GoMe exhibited stable photothermal property. Because the release kinetics of GoMe is super sensitive to the NIR irradiation, DOX@GoMe showed synergistic effect in killing cancer cell upon NIR irradiation. Since the first *in vitro* report of mesoporous silica-coated gold nanorod reported by Zhang et al.,[39] several recent studies explored its application for tumor growth inhibition *in vivo*.[40,41] However, none of them have been utilized for cancer detection. Due to the

abundance of PDA segments on the GNS, GoMe could be conveniently modified with DOTA and achieved excellent chelating capacity needed for PET imaging. To the best of our knowledge, GoMe is the first gold/mesoporous silica hybrid nano-system which is capable of both detecting clinically relevant spontaneous tumor and achieving the synergetic effect of photothermal therapy and chemotherapy in killing cancer cells. To further enhance the sensitivity of its cancer detection capacity and boost its anticancer efficacy, the next step research will incorporate tumor targeting ligands, such as RGD peptide, folic acid, and anisamide, which target cancer cells overexpressed integrins,[42] folate,[43,44] and sigma-2 receptors,[45,46] respectively, into GoMe.

5. Conclusion

In summary, a photothermal stable gold/mesoporous silica hybrid nanoparticle (GoMe), which possesses the merits of both conventional gold nanoparticles and mesoporous silica nanoparticles, such as good photothermal converting ability and high drug loading capacity, has been developed. In contrast to other MSN based system, GoMe is well dispersed in serum containing medium. Contrary to GNR and other heat generating gold nanoparticles, GoMe is stable in structure and maintains its photothermal converting capacity after repetitive NIR irradiation. The release of drug from GoMe can be triggered by both intracellularlly elevated redox potential and NIR irradiation. The localization of doxorubicin loaded GoMe can be detected by both fluorescence and dark-field microscopies. In addition, the combination of DOX@GoMe and NIR irradiation exhibited synergistic effect at the DOX concentration 5 μM through the integration of photothermal therapy and chemotherapy. Furthermore, PET imaging proved that GoMe is a good tool for the detection of clinically relevant spontaneous lung tumor. Based on these promising *in vitro* and *in vivo* results, further studies will focus on the pharmacokinetics of GoMe and utilizing it as an effective tool for image-guided cancer therapy.

Acknowledgments

The authors want to thank the ASPIRE award from the Office of the Vice President for Research of The University of South Carolina, the National Cancer Institute (CCSG P30 CA44579 and 1R15CA188847-01A1), and the Center for Targeted Therapeutics (5P20GM109091-02) for financial support. We also want to thank Dr. Feng Gao for his help in the live and dead cell staining, Dr. Linda Shimizu for the TGA assay, Dr. Natalia B. Shustova for the BET measurement, and Dr. Xinyu Huang for the dark-field microscopy.

References

1. Khan MS, Vishakante GD, Siddaramaiah H. Gold nanoparticles: A paradigm shift in biomedical applications. Adv Colloid Interface Sci. 2013; 199–200:44–58.
2. Skrabalak SE, Au L, Lu X, Li X, Xia Y. Gold nanocages for cancer detection and treatment. Nanomedicine. 2007; 2:657–668. [PubMed: 17976028]
3. Alkilany AM, Thompson LB, Boulos SP, Sisco PN, Murphy CJ. Gold nanorods: Their potential for photothermal therapeutics and drug delivery, tempered by the complexity of their biological interactions. Adv Drug Deliv Rev. 2012; 64:190–199. [PubMed: 21397647]
4. Stern JM, Stanfield J, Lotan Y, Park S, Hsieh JT, Cadeddu JA. Efficacy of laser-activated gold nanoshells in ablating prostate cancer cells in vitro. J Endourol. 2007; 21:939–943. [PubMed: 17867958]
5. Huang X, El-Sayed MA. Plasmonic photo-thermal therapy (PPTT). Alexandria J Med. 2011; 47:1–9.

6. Kwon KC, Ryu JH, Lee JH, Lee EJ, Kwon IC, Kim K, Lee J. Proteinticle/Gold Core/Shell Nanoparticles for Targeted Cancer Therapy without Nanotoxicity. Adv Mater. 2014; 26:6436–6441. [PubMed: 25044204]
7. Zhang Z, Wang J, Chen C. Near-infrared light-mediated nanoplatforms for cancer thermo-chemotherapy and optical imaging. Adv Mater. 2013; 25:3869–3880. [PubMed: 24048973]
8. Skrabalak SE, Chen J, Au L, Lu X, Li X, Xia Y. Gold Nanocages for Biomedical Applications. Adv Mater. 2007; 19:3177–3184. [PubMed: 18648528]
9. Dong W, Li Y, Niu D, Ma Z, Gu J, Chen Y, Zhao W, Liu X, Liu C, Shi J. Facile synthesis of monodisperse superparamagnetic Fe3O4 Core@hybrid@Au shell nanocomposite for bimodal imaging and photothermal therapy. Adv Mater. 2011; 23:5392–5397. [PubMed: 21997882]
10. Yavuz MS, Cheng Y, Chen J, Cobley CM, Zhang Q, Rycenga M, Xie J, Kim C, Song KH, Schwartz AG, Wang LV, Xia Y. Gold nanocages covered by smart polymers for controlled release with near-infrared light. Nat Mater. 2009; 8:935–939. [PubMed: 19881498]
11. Dickerson EB, Dreaden EC, Huang X, El-Sayed IH, Chu H, Pushpanketh S, McDonald JF, El-Sayed MA. Gold nanorod assisted near-infrared plasmonic photothermal therapy (PPTT) of squamous cell carcinoma in mice. Cancer Lett. 2008; 269:57–66. [PubMed: 18541363]
12. Loo C, Lin A, Hirsch L, Lee MH, Barton J, Halas N, West J, Drezek R. Nanoshell-enabled photonics-based imaging and therapy of cancer. Technol Cancer Res Treat. 2004; 3:33–40. [PubMed: 14750891]
13. Link S, Burda C, Nikoobakht B, El-Sayed MA. Laser-Induced Shape Changes of Colloidal Gold Nanorods Using Femtosecond and Nanosecond Laser Pulses. J Phys Chem B. 2000; 104:6152–6163.
14. Chen J, Wiley B, Li ZY, Campbell D, Saeki F, Cang H, Au L, Lee J, Li X, Xia Y. Gold Nanocages: Engineering Their Structure for Biomedical Applications. Adv Mater. 2005; 17:2255–2261.
15. Aguirre CM, Moran CE, Young JF, Halas NJ. Laser-Induced Reshaping of Metallodielectric Nanoshells under Femtosecond and Nanosecond Plasmon Resonant Illumination. J Phys Chem B. 2004; 108:7040–7045.
16. Xiao Y, Hong H, Matson VZ, Javadi A, Xu W, Yang Y, Zhang Y, Engle JW, Nickles RJ, Cai W, Steeber DA, Gong S. Gold Nanorods Conjugated with Doxorubicin and cRGD for Combined Anticancer Drug Delivery and PET Imaging. Theranostics. 2012; 2:757–768. [PubMed: 22916075]
17. Wu C, Yu C, Chu M. A gold nanoshell with a silica inner shell synthesized using liposome templates for doxorubicin loading and near-infrared photothermal therapy. Int J Nanomedicine. 2011; 6:807–813. [PubMed: 21589648]
18. Zhu Y, Meng W, Gao H, Hanagata N. Hollow Mesoporous Silica/Poly(l-lysine) Particles for Codelivery of Drug and Gene with Enzyme-Triggered Release Property. J Phys Chem C. 2011; 115:13630–13636.
19. Zhao W, Zhang H, He Q, Li Y, Gu J, Li L, Li H, Shi J. A glucose-responsive controlled release of insulin system based on enzyme multilayers-coated mesoporous silica particles. Chem Commun. 2011; 47:9459–9461.
20. Guo W, Wang J, Lee SJ, Dong F, Park SS, Ha CS. A General pH-Responsive Supramolecular Nanovalve Based on Mesoporous Organosilica Hollow Nanospheres. Chem Eur J. 2010; 16:8641–8646. [PubMed: 20593447]
21. Angelos S, Khashab NM, Yang YW, Trabolsi A, Khatib HA, Stoddart JF, Zink JI. pH Clock-Operated Mechanized Nanoparticles. J Am Chem Soc. 2009; 131:12912–12914. [PubMed: 19705840]
22. Meng H, Xue M, Xia T, Zhao YL, Tamanoi F, Stoddart JF, Zink JI, Nel AE. Autonomous in Vitro Anticancer Drug Release from Mesoporous Silica Nanoparticles by pH-Sensitive Nanovalves. J Am Chem Soc. 2010; 132:12690–12697. [PubMed: 20718462]
23. Aznar E, Marcos MD, Martínez-Máñez R, Sancenón F, Soto J, Amorós P, Guillem C. pH- and Photo-Switched Release of Guest Molecules from Mesoporous Silica Supports. J Am Chem Soc. 2009; 131:6833–6843. [PubMed: 19402643]

24. Vivero-Escoto JL, Slowing II, Wu CW, Lin VSY. Photoinduced Intracellular Controlled Release Drug Delivery in Human Cells by Gold-Capped Mesoporous Silica Nanosphere. J Am Chem Soc. 2009; 131:3462–3463. [PubMed: 19275256]
25. Jana NR, Gearheart L, Murphy CJ. Seeding Growth for Size Control of 5–40 nm Diameter Gold Nanoparticles. Langmuir. 2001; 17:6782–6786.
26. Locke LW, Mayo MW, Yoo AD, Williams MB, Berr SS. PET imaging of tumor associated macrophages using mannose coated 64Cu liposomes. Biomaterials. 2012; 33:7785–7793. [PubMed: 22840225]
27. Wani A, Muthuswamy E, Savithra GHL, Mao GZ, Brock S, Oupicky D. Surface Functionalization of Mesoporous Silica Nanoparticles Controls Loading and Release Behavior of Mitoxantrone. Pharm Res. 2012; 29:2407–2418. [PubMed: 22555380]
28. Pattani VP, Tunnell JW. Nanoparticle-mediated photothermal therapy: A comparative study of heating for different particle types. Lasers Surg Med. 2012; 44:675–684. [PubMed: 22933382]
29. Jana NR, Gearheart L, Murphy CJ. Wet Chemical Synthesis of High Aspect Ratio Cylindrical Gold Nanorods. J Phys Chem B. 2001; 105:4065–4067.
30. Ganta S, Devalapally H, Shahiwala A, Amiji M. A review of stimuli-responsive nanocarriers for drug and gene delivery. J Control Release. 2008; 126:187–204. [PubMed: 18261822]
31. Meng FH, Hennink WE, Zhong Z. Reduction-sensitive polymers and bioconjugates for biomedical applications. Biomaterials. 2009; 30:2180–2198. [PubMed: 19200596]
32. Bae Y, Fukushima S, Harada A, Kataoka K. Design of environment-sensitive supramolecular assemblies for intracellular drug delivery: Polymeric micelles that are responsive to intracellular pH change. Angew Chem Int Ed. 2003; 42:4640–4643.
33. Shen J, He Q, Gao Y, Shi J, Li Y. Mesoporous silica nanoparticles loading doxorubicin reverse multidrug resistance: performance and mechanism. Nanoscale. 2011; 3:4314–4322. [PubMed: 21892492]
34. Lu J, Liong M, Zink JI, Tamanoi F. Mesoporous Silica Nanoparticles as a Delivery System for Hydrophobic Anticancer Drugs. Small. 2007; 3:1341–1346. [PubMed: 17566138]
35. Chou TC. Drug Combination Studies and Their Synergy Quantification Using the Chou-Talalay Method. Cancer Res. 2010; 70:440–446. [PubMed: 20068163]
36. Lee D, Hong JW, Park C, Lee H, Lee JE, Hyeon T, Paik SR. Ca2+-Dependent Intracellular Drug Delivery System Developed with “Raspberry-Type” Particles-on-a-Particle Comprising Mesoporous Silica Core and α-Synuclein-Coated Gold Nanoparticles. ACS Nano. 2014; 8:8887–8895. [PubMed: 25166911]
37. Sharma P, Brown SC, Bengtsson N, Zhang Q, Walter GA, Grobmyer SR, Santra S, Jiang H, Scott EW, Moudgil BM. Gold-Speckled Multimodal Nanoparticles for Noninvasive Bioimaging. Chem Mater. 2008; 20:6087–6094. [PubMed: 19466201]
38. Lin M, Guo C, Li J, Zhou D, Liu K, Zhang X, Xu T, Zhang H, Wang L, Yang B. Polypyrrole-Coated Chainlike Gold Nanoparticle Architectures with the 808 nm Photothermal Transduction Efficiency up to 70%. ACS Appl Mater Interfaces. 2014; 6:5860–5868. [PubMed: 24660754]
39. Zhang Z, Wang L, Wang J, Jiang X, Li X, Hu Z, Ji Y, Wu X, Chen C. Mesoporous Silica-Coated Gold Nanorods as a Light-Mediated Multifunctional Theranostic Platform for Cancer Treatment. Adv Mater. 2012; 24:1418–1423. [PubMed: 22318874]
40. Terentyuk G, Panfilova E, Khanadeev V, Chumakov D, Genina E, Bashkatov A, Tuchin V, Bucharskaya A, Maslyakova G, Khlebtsov N, Khlebtsov B. Gold nanorods with a hematoporphyrin-loaded silica shell for dual-modality photodynamic and photothermal treatment of tumors in vivo. Nano Res. 2014; 7:325–337.
41. Shen S, Tang H, Zhang X, Ren J, Pang Z, Wang D, Gao H, Qian Y, Jiang X, Yang W. Targeting mesoporous silica-encapsulated gold nanorods for chemo-photothermal therapy with near-infrared radiation. Biomaterials. 2013; 34:3150–3158. [PubMed: 23369218]
42. Bahadur KCR, Xu P. Multicompartment Intracellular Self-Expanding Nanogel for Targeted Delivery of Drug Cocktail. Adv Mater. 2012; 24:6479–6483. [PubMed: 23001909]
43. Shen Y, Zhou Z, Sui M, Tang J, Xu P, Van Kirk EA, Murdoch WJ, Fan M, Radosz M. Charge-reversal polyamidoamine dendrimer for cascade nuclear drug delivery. Nanomedicine (UK). 2010; 5:1205–1217.

44. Hilgenbrink AR, Low PS. Folate receptor-mediated drug targeting: From therapeutics to diagnostics. J Pharm Sci. 2005; 94:2135–2146. [PubMed: 16136558]

45. Yang Y, Hu YX, Wang YH, Li J, Liu F, Huang L. Nanoparticle Delivery of Pooled siRNA for Effective Treatment of Non-Small Cell Lung Caner. Mol Ther. 2012; 9:2280–2289.

46. He H, Cattran AW, Nguyen T, Nieminen AL, Xu P. Triple-responsive expansile nanogel for tumor and mitochondria targeted photosensitizer delivery. Biomaterials. 2014; 35:9546–9553. [PubMed: 25154666]

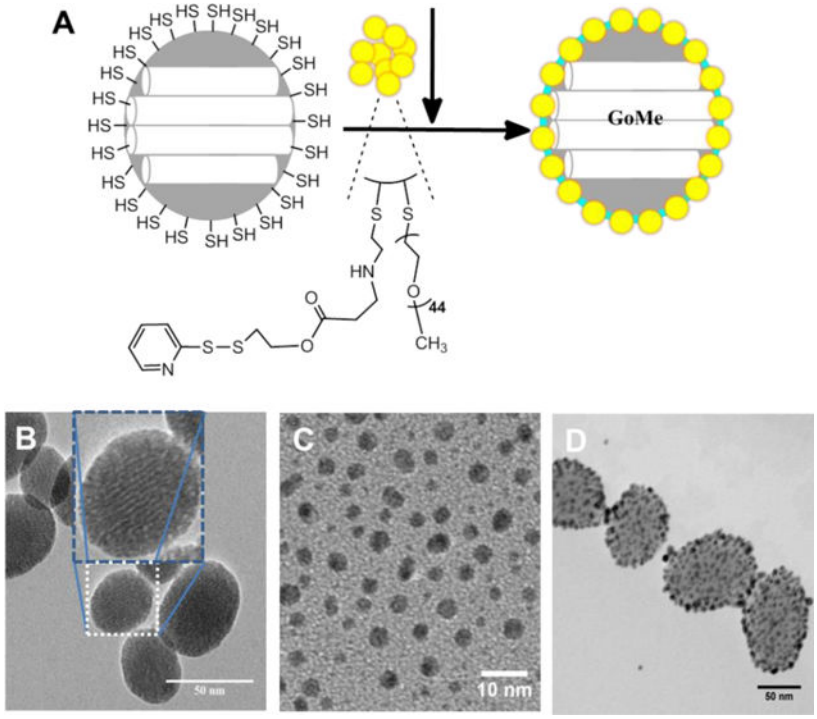

Figure 1.

(A) Schematic illustration of the fabrication of GoMe, and TEM images of MSN (B), PEG-GNS (C), and GoMe nanoparticles (D). Scale bars are 50, 10, and 50 nm in (B), (C), and (D), respectively. The inset in (B) shows the TEM image of one individual MSN.

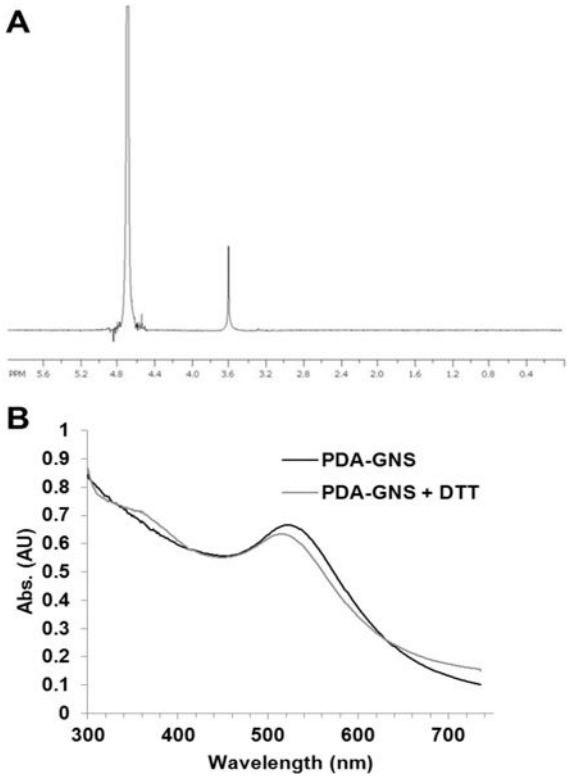

Figure 2.
^{1}H-NMR of PEG-GNS in D2O (A) and the UV-Vis spectra of PDA-GNS (B).

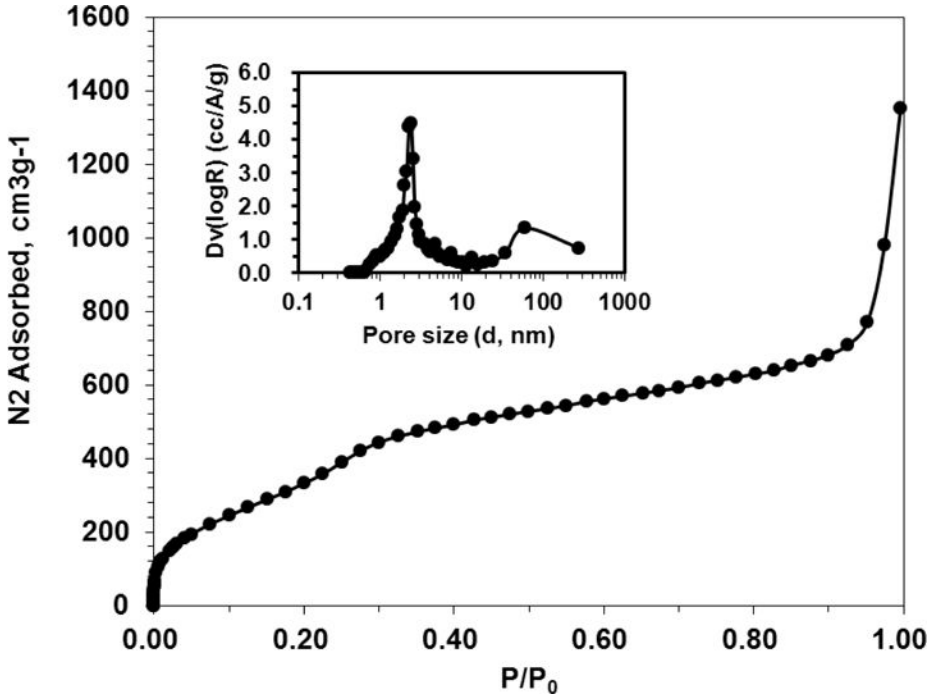

Figure 3.
Nitrogen sorption isotherm for MSN. The insert shows the pore size distribution.

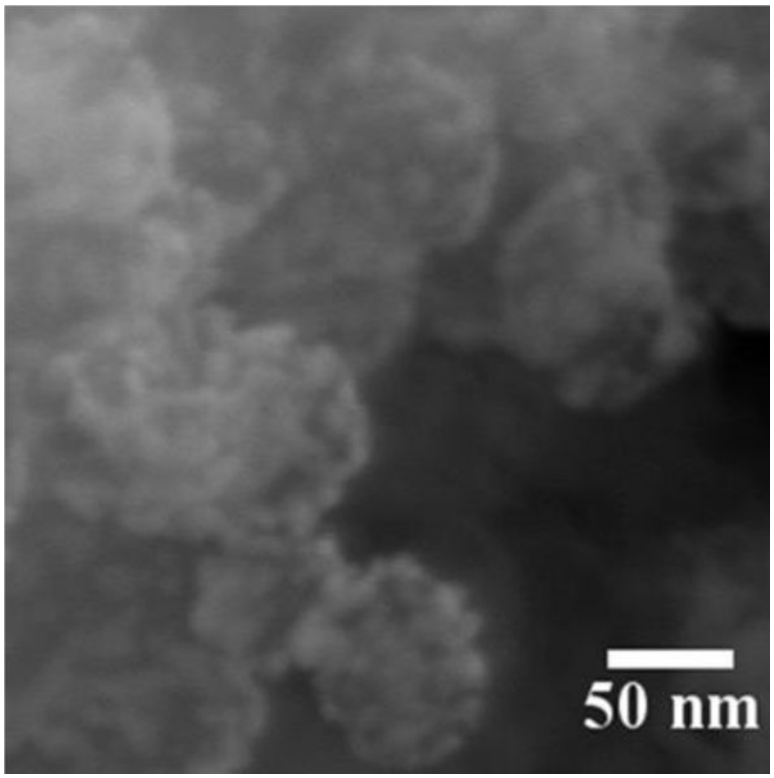

Figure 4.
SEM image of GoMe. Image was acquired with a Zeiss Ultra Plus FESEM at the magnification of 300,000 ×.

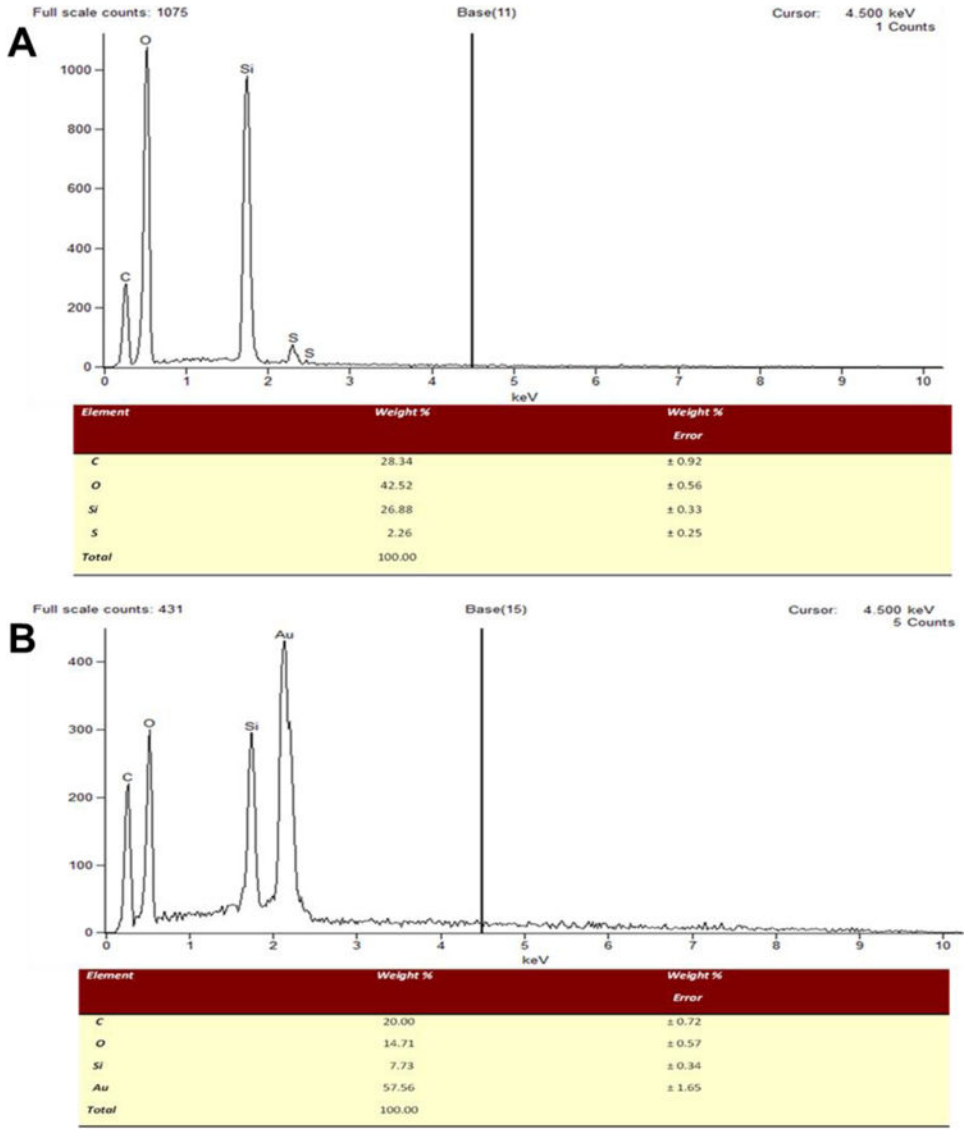

Figure 5.
SEM-EDX analysis of MSN-SH (A) and GoMe (B).

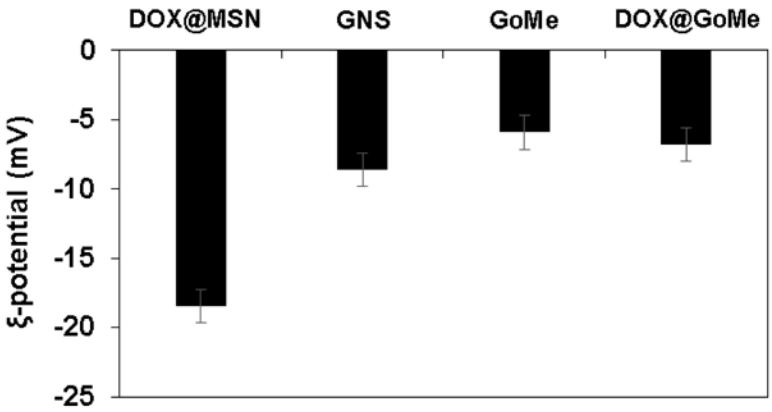

Figure 6.
The surface charge of MSN, GNS, GoMe, and DOX@GoMe.

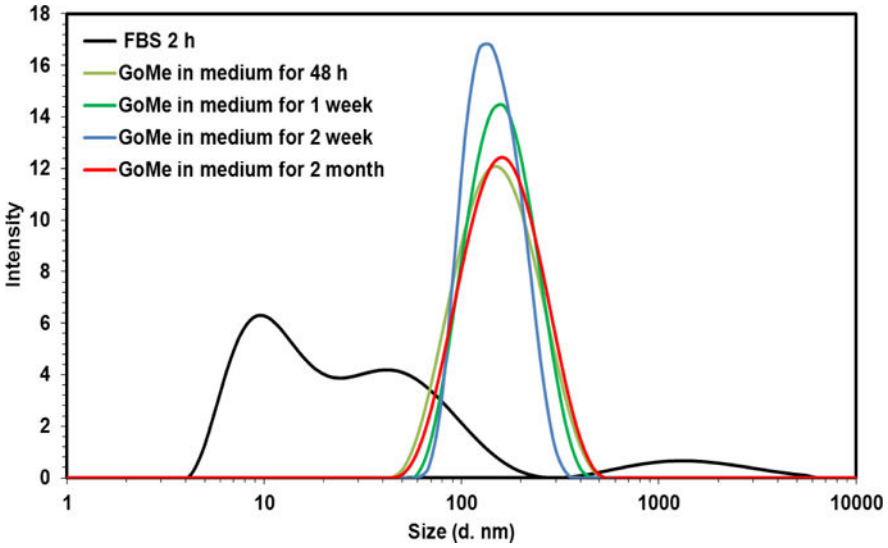

Figure 7.
Size distribution of GoMe in cell culture medium supplemented with 10% FBS.

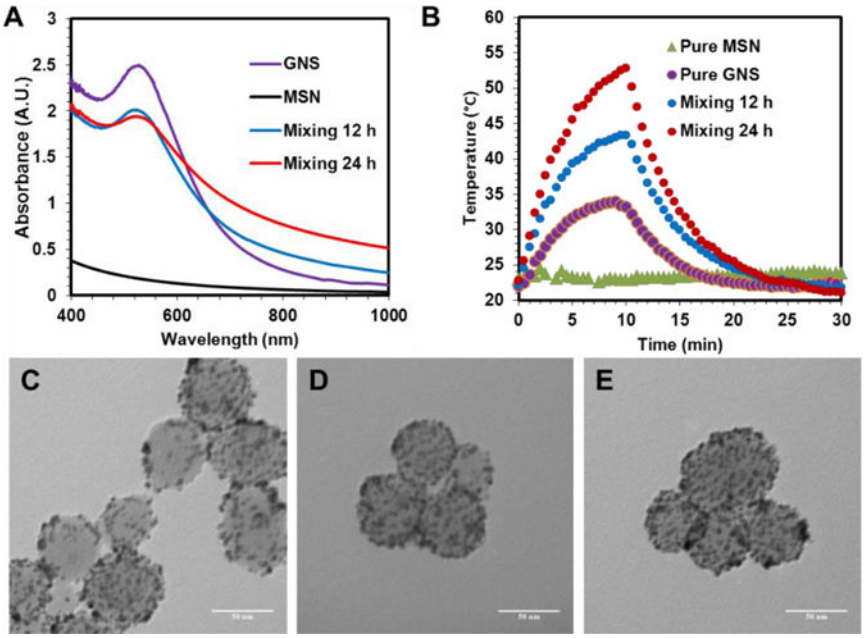

Figure 8.

The UV-Vis spectra of GNS, MSN, and their mixture after 12 and 24 h of reaction (A), as well as their photothermal heating curves upon 10 min of 808 nm laser irradiation (2.83 W/cm^2) (B). TEM images of GoMe formed after 2 (C), 12 (D), and 24 h (E) of mixing GNS and MSN. Scale bars are 50 nm in (C), (D), and (E).

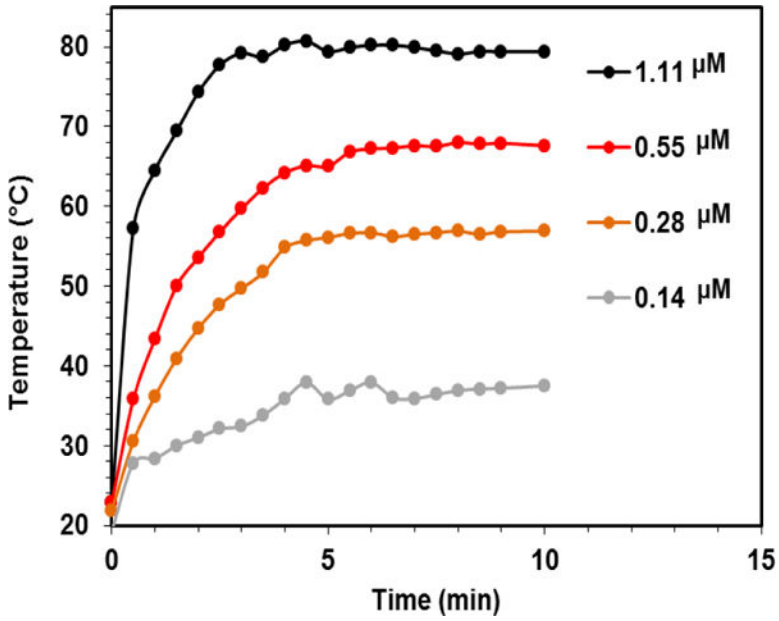

Figure 9.

The photothermal effect of GoMe at different concentrations (calculated based on GNS) at fixed GNS decorating density. Nano-suspension of GoMe was irradiated by a 808 nm laser (2.83 W/cm^2).

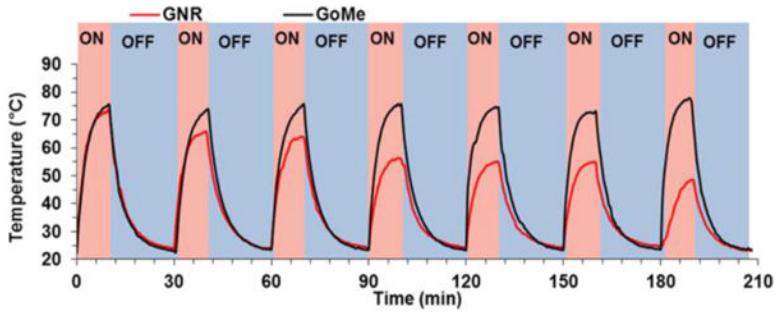

Figure 10.

Real-time temperature elevation of GoMe and GNR nano-suspensions during 7 cycles of NIR irradiation. GoMe and GNR were irradiated with a 808 nm NIR laser for 10 min (2.83 W/cm^2) and then cooled down for 20 min. The last cycle was carried out 24 h after the 6th cycle.

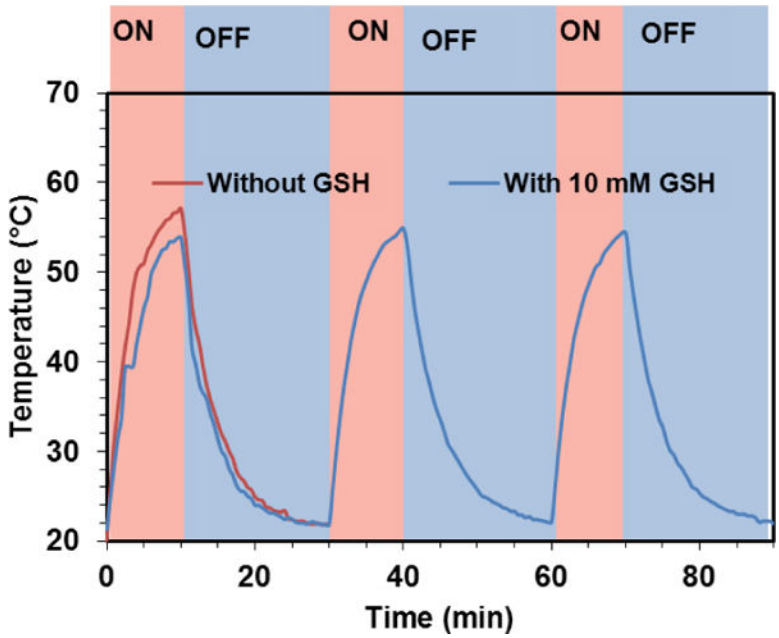

Figure 11.

The photothermal effect of GoMe in medium with or without 10 mM GSH. Nano-suspension of GoMe was irradiated by a 808 nm laser (2.83 W/cm^2, 10 min on and 20 min off).

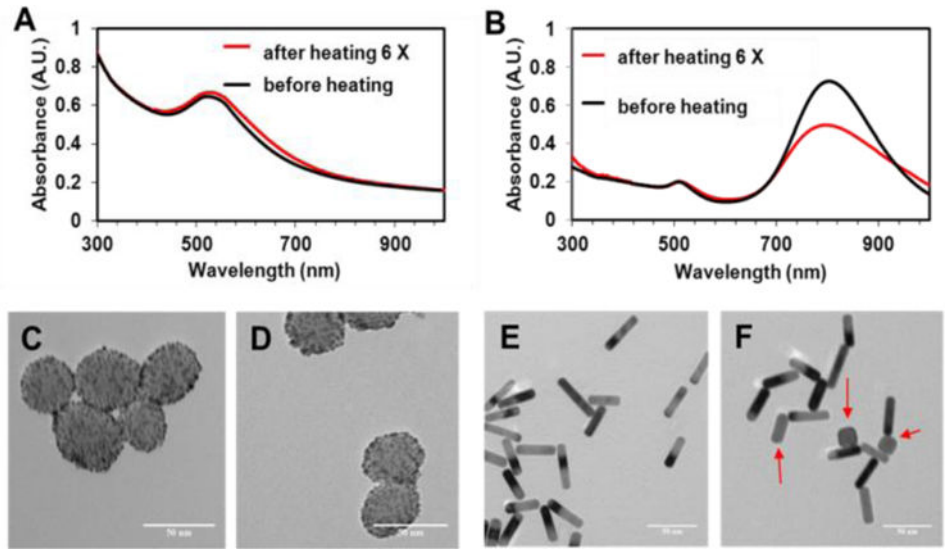

Figure 12.

The UV-Vis spectra (A) and TEM images of GoMe (C, D), and the UV-Vis spectra (B) and TEM images of GNR (E, F). TEM images of GoMe before laser irradiation (C) and after 5 cycles of irradiation induced heating/cooling (D). TEM images of GNR before laser irradiation (E) and after 5 cycles of irradiation induced heating/cooling (F). Red arrows indicate those GNRs changed to round shape (F). Scale bars are 50 nm in all images.

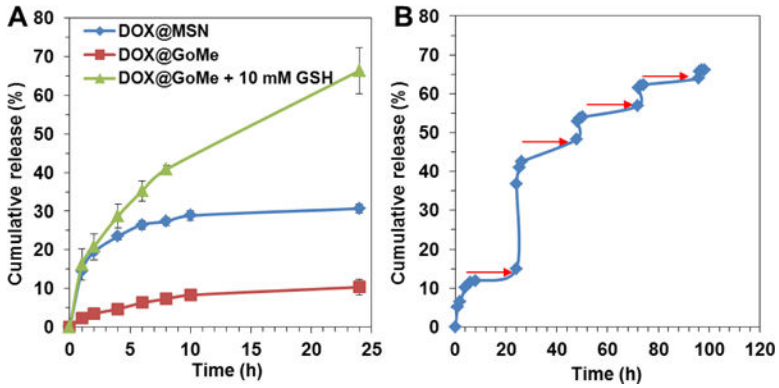

Figure 13.

The release kinetics of GoMe in plain PBS or PBS supplemented with GSH (A) and under the trigger of NIR irradiation (B). The red arrows indicate the time points when the irradiation (10 min, 2.83 W/cm^2) was applied. Data were presented as mean ± SD, n=3.

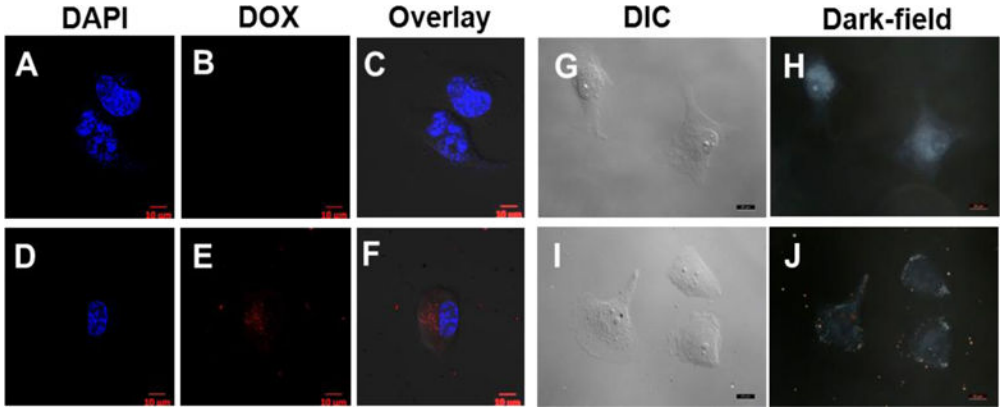

Figure 14.

The confocal (A–F) and dark-field (G–J) images of A2058 cells co-cultured with DOX@GoMe. Cells in A–C, and G–H were control. Cells in D–F, and I–J were treated with DOX@GoMe. Images H and J were collected in dark-field mode. Scale bars in A–J are 10 μm.

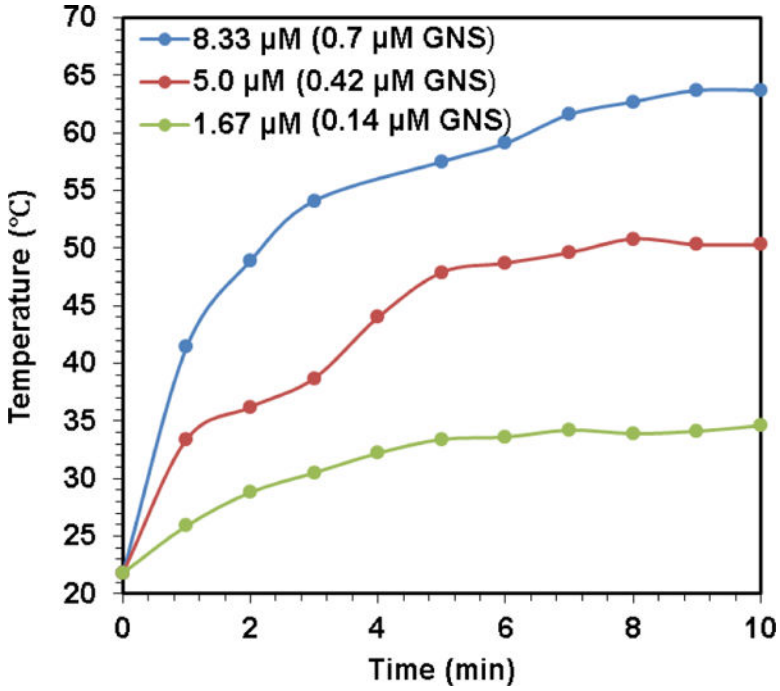

Figure 15.

The real-time medium temperature during NIR laser irradiation of different GoMe concentrations (calculated based on corresponding DOX concentration).

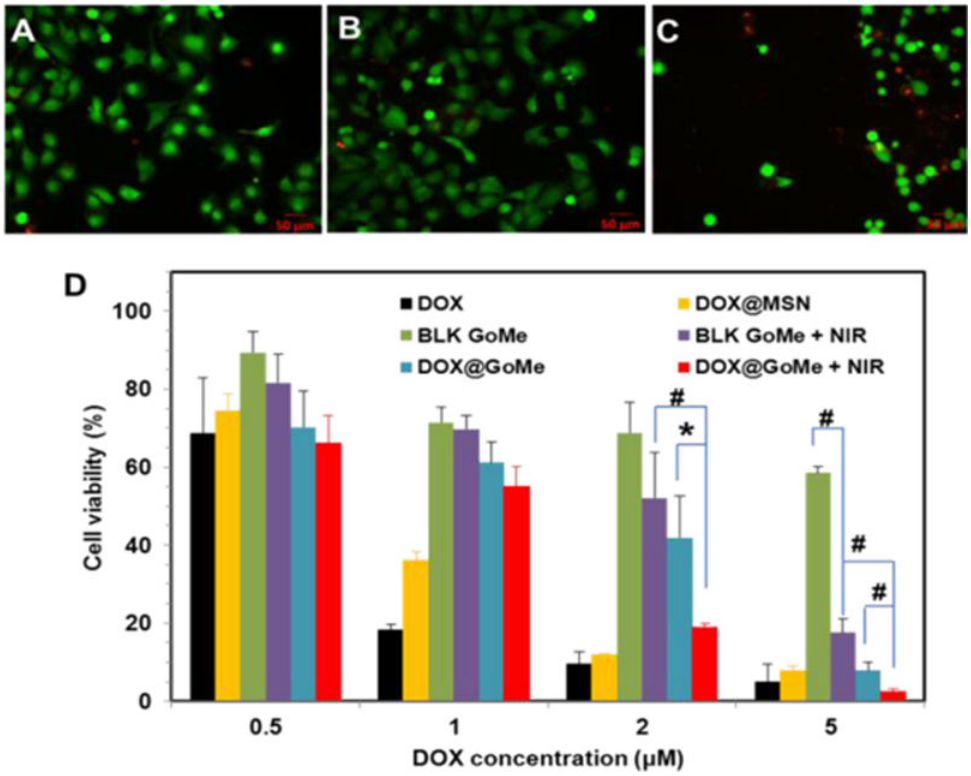

Figure 16.

The fluorescent images of live/dead cell assay (A–C) after NIR irradiation and the cytotoxicity of DOX@GoMe coupled with NIR irradiation (D). Cells in A, B, and C were treated with blank medium, blank GoMe, and GoMe coupled with NIR irradiation, respectively. The laser dose was 10 min, 2.83 W/cm^2. Scale bars in A–C are 50 μm. Data were presented as mean ± SD, n=3, $P < 0.05$ *; $P < 0.01$ $^{\#}$).

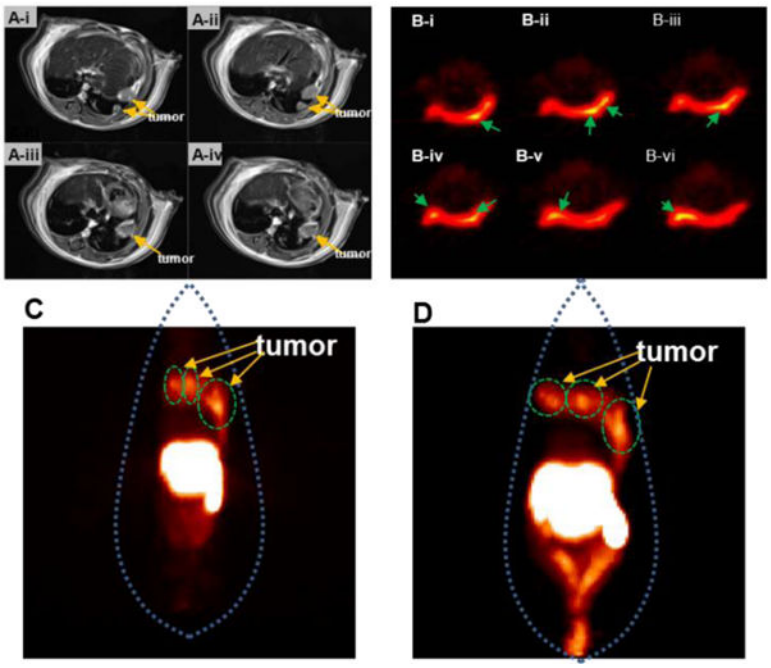

Figure 17.

(A) Four contiguous MRI transverse images, (B–D) PET images of 3 tumors in the lung of mouse received radiolabeled GoMe. Tumors are indicated by yellow arrows in (A). (B) PET images of contiguous slices in transverse acquired 6 h post administration. Tumors are indicated by green arrows in (B). Whole body PET images acquired 6 h (C) and 20 h (D) post administration.